

Froude characterisation for single-surge unsteady dry granular flows:
impact pressure and runup height

2019/02/22

General information of the article

Type of paper: Article

Title: Froude characterisation for single-surge unsteady dry granular flows: impact pressure and runup height

Authors: C. W. W. Ng, C.E. Choi* and G. R. Goodwin

Author information:

Lead author: C. W. W. Ng

Chair Professor, Department of Civil and Environmental Engineering, Hong Kong University of Science and Technology, Clear Water Bay, Kowloon, Hong Kong.

E-mail: cecwwng@ust.hk

Co-author*: C. E. Choi

Research Assistant Professor, Department of Civil and Environmental Engineering, and Institute for Advanced Study, Hong Kong University of Science and Technology, Clear Water Bay, Kowloon, Hong Kong.

E-mail: ceclarenc@ust.hk

Co-author: G. R. Goodwin

PhD candidate, Department of Civil and Environmental Engineering, Hong Kong University of Science and Technology, Clear Water Bay, Kowloon, Hong Kong

E-mail: rggoodwin@connect.ust.hk

* Corresponding author

Word count: 3834

Figures: 8 (main text) + 1 (appendix)

Tables: 2

Froude characterisation for single-surge unsteady dry granular flows: impact pressure and runup height

C. W. W. Ng¹, C. E. Choi^{1 2 3 *} and G. R. Goodwin¹

The Department of Civil and Environmental Engineering; The Hong Kong University of Science and Technology, Hong Kong ¹

The HKUST Jockey Club Institute for Advanced Study, Hong Kong ²

HKUST Fok Ying Tung Graduate School, Nansha, Guangzhou, China ³

Corresponding author *

Abstract

The impact and pileup mechanisms of unsteady granular flows impacting a rigid barrier are governed by the Froude conditions (Fr). Velocity and depth vary along the length of the flow. There is currently no widely-accepted approach for characterising Fr for impact and runup problems. In this study, a Discrete Element Method (DEM) model was calibrated against a physical flume test. 86 simulations were performed using the DEM model to investigate the equivalent Fr governing pileup height and impact pressure for unsteady single-surge dry granular flows against a rigid barrier. Fr and the grain diameter were varied. Results reveal that Fr within the frontmost 5% of a flow governs both pileup height and impact pressure. Thus, taking frontal velocity and maximum flow depth within the frontmost region is crucial for properly characterising the runup height and impact load. Consistent characterisation of Fr is possible near the longitudinal centre of a flow; the frontmost Fr can then be extrapolated from calibration curves. Results imply that existing studies which predict impact pressure based on non-frontal Fr values may underestimate impact pressure by a factor of up to two.

Keywords: Granular flow; Froude; Flume modelling; DEM; impact; runup

List of notation

B	Width of channel	(m)
e	Coefficient of restitution	
F	Impact force	(kg m/s ²)
Fr	Froude number	
Fr_{\max}	Maximum Froude number	
Fr_{\min}	Minimum Froude number	
g	Acceleration due to the Earth's gravity	(m/s ²)
h	Flow depth	(m)
h_u	Upstream flow depth	(m)
h_d	Downstream flow depth (at barrier)	(m)
h_1	Height from which grain is dropped	(m)
h_2	Height to which grain rebounds	(m)
h_{\max}	Maximum upstream flow depth	(m)
L	Longitudinal position along flow	(m)
L_s	Length of measuring volume	(m)
N	Number of grains	
t	Time	(s)
U	Upstream flow velocity	(m/s)
\bar{U}	Depth-averaged upstream flow velocity	(m/s)
δ	Particle size	(m)
θ	Channel inclination	(°)
v	Solid volume fraction	
ρ	Bulk density	(kg/m ³)
ρ_m	Material density	(kg/m ³)
ρ_u	Upstream bulk density	(kg/m ³)
ρ_d	Downstream bulk density	(kg/m ³)
α	Coefficient for impact pressure equation	
ϕ'	Internal friction angle of granular material	

Introduction

Flow-type landslides threaten mountainous regions worldwide (e.g. Hungr et al. 2001; Sassa and Wang 2005; Arattano et al. 2012). Structural mitigation measures such as rigid barriers (Jiang and Towhata 2013) and slit-structures (VanDine 1996; Armanini and Larcher 2001) prevent flows from damaging downstream facilities. To guide the design of mitigation measures, the Froude conditions Fr (e.g. Hübl et al. 2009; Armanini *et al.* 2011; Cui *et al.* 2015; Ashwood and Hungr 2016) are used to characterise flows:

$$Fr^2 = \frac{U^2}{gh} \quad (1)$$

where U is velocity, g is acceleration due to the Earth's gravity, and h is flow depth. Fr represents the inertial state of a continuum with respect to an external field (in this case, the Earth's gravity). For open-channel granular flows, Fr can be invoked to differentiate between inertial and gravitational behavior and compare flows at different scales for dynamic similarity. Flows are dominated by inertial force for $Fr > 10$, gravity for $Fr < 0.1$, and a mixture of the two for $0.1 < Fr < 10$ (Faug 2015). Of course, other pertinent considerations include the solid volume fraction (Armanini et al. 2011, 2014; Armanini 2015) and the ratio between grain diameter and flow depth δ/h (Armanini 2015).

Fr governs the pileup height and impact pressure for flows impacting structures (Hübl et al. 2009; Armanini et al. 2011; Cui et al. 2015; Choi et al. 2015). Hákonardóttir et al. (2003) proposed an equation for granular flows impacting a rigid barrier considering a shockwave upstream:

$$2Fr^2 = \frac{\rho_d (h_d)^2}{\rho_u (h_u)} - \frac{h_d}{h_u} + \left(\frac{\rho_d h_d}{\rho_u h_u} \right)^{-1} - 1 \quad (2)$$

where ρ is density and subscripts u and d indicate 'upstream' and 'downstream' respectively. Eqn. 2 accounts for change in flow depth and density after impact. Impact pressure is most commonly estimated using the hydrodynamic approach (Eqn. 3), because of its simplicity and because its parameters are easy to obtain (Hübl et al. 2009):

$$P = \alpha \rho U^2 \quad (3)$$

where α is a coefficient accounting for the assumptions and simplifications made in Eqn. 3. A value of unity for α indicates the momentum of the flow is completely lost upon impact, while a value of two assumes the momentum rebounds in the opposite direction at an equal magnitude. In engineering practice, values quoted for α may also incorporate variation in impact pressure due to barrier flexibility or peculiarities of flow composition to ensure a conservative design (Ng et al. 2017). The right-hand-side, sans α , is the numerator of Fr . An alternative equation for impact force incorporating the effects of density and depth change, as well as an upstream shockwave, was proposed by Albaba et al. (2018). Eqn. 4 is a slightly simplified form thereof (with coefficients equal to unity not written):

$$P = \frac{F}{h_u B} = \left[1 + \frac{1}{\frac{\rho_d h_d}{\rho_u h_u} - 1} + \frac{1}{2Fr^2} \right] \rho_u \bar{U}_u^2 + \frac{1}{2} \left[\tan(\theta - \varphi') \frac{\rho_d h_d^2}{\rho_u h_u^2} \right] \rho_u g h_u \cos \theta \quad (4)$$

where B is the channel width; \bar{U} is the depth-averaged velocity; θ is the channel inclination; and φ' is the internal friction angle of the granular material. Notably, Fr appears directly.

A challenge for engineers is that many flow-type landslides are unsteady, having a wedge-shaped front (e.g. Gray et al. 2003; Choi et al. 2015, 2016) (Fig. 1). Quantities that affect Fr such as U and h thus vary longitudinally, causing Fr to vary; indeed, Fr is infinite at the tips and decreases towards the centre of the flow. The Froude number affects both the runup height and the impact pressure on a barrier. However, researchers fail to agree on what part of the flow is the most relevant for characterizing the runup height or impact pressure.

Choi et al. (2014a) characterized the Froude conditions for open channel sand flows before carrying out a series of scaled experiments to determine the effectiveness of baffle arrays (Choi et al. 2014a; 2014b) at reducing flow energy. The flow depth was taken as the maximum registered by an overhead laser sensor, whilst the flow velocity

was taken as the maximum from the frontal wedge obtained from Particle Imaging Velocimetry (White et al. 2003). Cui et al. (2015) characterized the Froude conditions for flows comprising a mixture of solids and liquids at an unspecified point somewhere in the flow front. The method used was similar to that of Choi et al. (2015). (The goal of the experiments was to determine force distribution on a single instrumented baffle; it was found that larger particles tend to gather at the flow head.)

In contrast to the previous two studies, Choi et al. (2016) took the depth-averaged velocity at the thickest part of the flow to determine the Froude conditions, before carrying out a series of tests investigating dry granular flows impacting a slit-dam. A range of channel inclinations were investigated; it was found Fr governed several aspects of interaction between the flow and slit-dam (e.g. the pileup height at the slit-dam). Eu et al. (2017) characterized the velocity and flow depth for mixed open-channel flows using cameras facing different directions; the point within the flows at which these quantities were measured was not specified. Vagnon and Segalini (2016) determined the flow depth before a rigid barrier using ultrasound sensors. The flow velocity was back-calculated from the time interval between the ultrasound sensors detecting flow material and the rigid barrier detecting impact. The velocity and depth were thus not determined in the same position, and the point on the wedge at which the depth was calculated was not stated. Scheidl et al. (2013) characterized Froude conditions for both laboratory-scale and prototype flows based on the maximum surface velocity and maximum flow thickness, which are unlikely to have occurred at the same point. (The goal of the study was to study the pressure distribution on a rigid structure due to flows comprising both solids and liquids; existing impact models were evaluated as a result of the research.)

Other estimates of Fr for prototype flows (e.g. Hübl et al. 2009; Proske et al. 2011) suffer from a similar lack of clear characterisation criteria, so it is difficult to meaningfully make comparisons between studies.

This manuscript aims to determine what characterisation criteria should be adopted for flows. A Discrete Element Model (DEM) is calibrated against a physical flume test using dry granular material. The DEM implementation used is LIGGGHTS

(Kloss and Goniva 2010; Law 2015). The results from eighty-four open-channel and two rigid barrier simulations are presented. The channel inclination is varied to alter Fr . Using the computed impact force, as well as the final flow depth and density, the equivalent Fr are back-calculated using Eqns. (2) to (4), to determine an appropriate method for characterising Fr . Since grain diameter is also important for open-channel flow dynamics (Armanini 2015), a parametric study on the influence of grain diameter on Fr is then carried out.

Physical and numerical modelling

A physical test was carried out using a flume with dimensions of $6.0 \times 0.2 \times 0.5$ m (length \times width \times depth) (Choi et al. 2016) (Fig. 2). Uniformly-sized glass spheres were inserted into a storage section at the upstream end of the flume. A spring-loaded gate retained material until dam-break. The dimensions of the numerical model were identical to the physical one, with the flume boundaries and gate modelled as rigid planes.

Model preparation and testing procedures: physical tests

A total mass of 40 kg of glass spheres was inserted into the storage area. Where appropriate, the barrier was installed inside the flume 900 mm downstream from the gate. The flume was then inclined using an overhead crane. A high-speed Prosilica GE640 camera facing the side-wall of the flume, filming at 300 FPS and at a resolution of 1500 by 1000 pixels, was initiated. The gate was then opened.

Model preparation and testing procedures: DEM tests

In the DEM model, a single rigid plane was used to model the rigid barrier (Fig. 2b). Discrete elements were generated randomly inside the storage area and allowed to settle. The number of grains N was similar to that of those in the physical experiments. N was back-calculated based on the radius of the grains, their density as well as their total mass:

$$N = \frac{\text{combined volume of all grains}}{\text{volume of individual grain}} = \frac{M/\rho}{\pi\delta^3/6} \quad (5)$$

After the system came to rest, the direction of gravity was rotated to simulate inclining the flume. The system was again allowed to come to rest. The gate then swung open, allowing material to flow downstream. Table 1 summarises DEM input parameters; the Appendix details how the coefficient of restitution was characterised. The friction angle between the particles and boundaries was characterised in Choi et al. (2016), whilst the inter-grain friction angle was treated as the lone unknown parameter for the DEM simulations. A coefficient of 0.36 was found to give an acceptable match between physical and simulated data.

Computation of flow properties

The *Froude conditions* Fr for the open-channel numerical simulations were obtained from a measuring volume located 0.8 m downstream. The dimensions of this measuring volume were 0.1 by 0.2 m (downstream by cross-stream). At each timestep, a value of Fr was calculated for each grain within the (stationary) volume, and an average of all the grains within the volume was then taken:

$$Fr = \frac{1}{N} \sum_{i=1}^N \frac{U_i}{\sqrt{gh_i}} \quad (6)$$

where N is the number of grains in the measuring volume. The vertical position of each grain was adopted as the height h_i . For the tests including the rigid barrier, the pileup height was calculated as double the mean height of the grains:

$$h_d = \frac{2}{N} \sum_{i=1}^N h_i \quad (7)$$

The pileup height was measured using a measuring volume placed directly upstream of the closed rigid barrier. The measuring volume was infinitely tall and wide, and had a length of 50 mm in the longitudinal direction to ensure a sufficiently large sample of grains were considered. The solid volume fraction was obtained using Eqn. (8a); the bulk density ρ (either upstream, ρ_u , or downstream, ρ_d) was obtained using Eqn. (8b):

$$v_s = \frac{N\pi\delta^3}{6L_s h B} \quad (8a)$$

$$\rho = v_s \rho_m \quad (8b)$$

where L_s is the length of the measuring volume. Pressure on the barrier was extracted from the reaction force on the barrier itself, so the measuring volume for pressure enveloped just the upstream face of the barrier. Pressure was calculated at each timestep as:

$$P = \frac{1}{h_d B} \sum_{i=1}^N F_i \quad (9)$$

where h_d is the depth of the impacting flow, B is the width of the channel and F_i is the force measured on the closed rigid barrier.

Test programme

A physical test at an inclination of 30° with a rigid barrier was performed. Two DEM simulations with a rigid barrier (at 14° and 30°) and four in an open channel (at 14° , 22° , 30° and 38°) were performed using spheres of diameter 10 mm. A further 80 simulations were run using grain diameters from 12 to 50 mm for the same four channel inclinations. Table 2 summarises the test programme.

Calibration: Comparison of physical and computed flow kinematics

Fig. 3 shows a comparison of the observed (left) and computed (right) flow kinematics. The purpose of this exercise was to assess the reliability of the DEM simulation. Specifically, the ability of the DEM model to capture the impact kinematics and pileup height was assessed. Load cells were not installed on the barrier, so a direct comparison of pressure obtained from the physical experiment and DEM simulations was not made.

Time $t = 0.0$ s (Fig. 3a) shows the flow approaching the barrier. The flow is wedge-shaped (e.g. Gray et al. 2003; Cagaeo 2014; Choi et al. 2015, 2016). The flow has impacted the barrier at $t = 0.2$ s (Fig. 3b) and runs up the barrier (Choi et al. 2015, 2016). From $t = 0.4$ to 0.8 s (Figs. 3c to 3e), pileup develops in front of the barrier, with the profile of the flow becoming progressively triangular. The impact kinematics are qualitatively matched by the numerical simulation at each time-step, lending confidence to the input parameters adopted.

Interpretation of results

Evolution of Froude conditions for open-channel flows

Fig. 4a shows Fr (ordinate) along the length of an open-channel flow L (abscissa, where zero and unity indicate the flow head and tail respectively). Four channel inclinations are shown: 14, 22, 30 and 38°. Reference regions demarcating supercritical Fr and a transition region (Faug 2015) are also shown.

The Froude conditions increase with channel inclination (Choi et al. 2015, 2016) along the entire length of the flow. Increasing the channel inclination causes a larger conversion of gravitational potential energy to kinetic energy per horizontal unit length, thus increasing the numerator of Fr . Furthermore, for all channel inclinations, Fr drops sharply along the first 10% of the flow. For $\theta = 38^\circ$, Fr drops from 16 to 8 over this distance, a reduction of 50%. A similar reduction is observed for the other inclinations. The drastic drop is attributed to the wedge-shape profile of the flow front.

Fr levels off for all four inclinations at about $L = 0.25$, and a minimum is reached near the longitudinal centre ($L = 0.5$). At the longitudinal centre, the depth-averaged velocity tends to be at a minimum. Fr gradually increases near the tail of the flow ($0.75 < L < 1$), because the flow tail tends to thin out.

Flow density affects both pileup height (Eqn. 2; Hákonardóttir et al. 2003) and impact pressure (Eqn. 3; Albaba et al. 2017). Fig. 4b shows the solid volume fraction and bulk density on the ordinate and L on the abscissa. The decrease in Fr observed along the front of the flow (Fig. 4a) is accompanied by an increase in the bulk density. This suggests that the impact pressure as calculated using Eqn. 3 may be subject to competition between varying Fr and ρ .

As Fr varies enormously along the length of the flow (L), values often quoted for Fr for different flows are unlikely to be directly comparable. Even a small variation in L at which velocity and flow depth are sampled can lead to a large difference in the Fr computed. Calculated predictions for pileup height and impact pressure (Eqns. 2 and

3) are potentially very inaccurate, necessitating a systematic approach for characterising Fr . The following sub-section shows the computed pressure, pileup height and density change for flows impacting a rigid barrier. Thereafter, both the value of Fr and the longitudinal position at which it occurs are back-calculated using computed pileup height and impact pressure.

Pressure, pileup height and density change for flows impacting a rigid barrier

Figs. 5a, 5b and 5c show the change in impact pressure, pileup height and bulk density (y-axis) with time (x-axis). These quantities are necessary to back-calculate Fr using Eqns. 2 to 4. Two sets of data are shown for channel inclinations of 14 and 30°.

Fig. 5a shows impact pressure. The inset is a zoomed-in version of the first 0.2 s of impact. Reference lines obtained from the hydrodynamic equation (Eqn. 3; Hübl et al. 2009) assuming α to be unity are also shown. The highest impact pressure is observed for both flows within the first 0.1 s. Several peaks are observed for both cases, similar to Cui et al. (2015) and Ng et al. (2017). Fig. 5b shows pileup height, as computed using Eqn. (7). The pileup height linearly increases for both flows, reaching a maximum height as the impact pressure reaches equilibrium. Fig. 5c shows the bulk density, which also reaches a maximum at the same time as the pileup depth.

Back-calculated Fr from pileup

Eqn. (2) includes the upstream Froude conditions Fr , the change in flow density ρ_d/ρ_u and the change in flow depth h_d/h_u after collision with the rigid barrier. The final pileup height h_d and final density ρ_d at the barrier were extracted using the calibrated Discrete Element Method model. Fr , ρ_u and h_u were extracted from an equivalent open-channel flow within the measuring volume at each timestep, and input into Eqn. (2). The part of the flow that provided the best fit with the measured pileup height was then determined. The data points were not gathered at the same time: data points corresponding to the front of the flow were obtained before data points at the tail, since the measuring volume was static.

Fig. 6 shows the predicted normalised pileup height on the y-axis and Fr on the x-axis. The predicted normalised pileup height comes from Eqn. (2), an analytic solution for the pileup height, using input parameters from the DEM. The supercritical and transitional regions are shown (Faug 2015). DEM data for inclinations of 14 and 30° are shown. The squares and crosses demarcate slices of the flow, each slice being 5% of the total flow length.

As shown in Fig. 4a, Fr is very large at the flow head, decreases towards a minimum in the centre of the flow and then tends to increase again at the tail. This trend can be seen for both channel inclinations. The initial increases in pileup height observed for both flows is due to the rapidly increasing flow density (Figs. 4b and 5c). The point at which Eqn. 2 best fulfils the measured pileup height (Fig. 5b) is marked with a red circle for each line. The circles both correspond to Fr of about 9, and both are found within the first 5% of the flow.

This implies that current methods for characterising Fr are unconservative and potentially dangerous. Adopting the maximum flow thickness and velocity to characterise Fr (as in Scheidl et al. 2014) would lead to values of Fr much smaller than at the flow front (Fig. 4a). This would lead to a severe underestimate of the pileup height calculated using Eqn. 2 (Hákonardóttir et al. 2003), causing potentially catastrophic overflow.

Back-calculated Fr from impact pressure

Figs. 7a and 7b show the normalised calculated impact pressure on a rigid barrier at each stage of an open-channel flow for channel inclinations of 30° and 14° respectively. The ordinate shows the calculated pressure (using Eqns. 3 and 4) normalised by that computed using the DEM (as per Eqn. 9). The abscissa shows Fr . The pressure was calculated thrice: using Eqn. 3b (Hübl et al. 2009), using α values of unity and two; and using Eqn. 4 (Albaba et al. 2017). A value of unity indicates the momentum of the flow is completely lost upon impact, while a value of two assumes the momentum rebounds in the opposite direction at an equal magnitude. Correspondingly, α of two is the theoretical upper bound. Of course, Eqn. 3b

assumes a homogenous and uniform flow, no frictional losses, and neglects the effects of gravity. Eqn. 4 considers density and height change during impact, as well as the formation of a shockwave that travels upstream. Markers are shown for each line and demarcate slices of the flow, as in Fig. 6. The arrows indicate progression from the head of the flow to the tail.

In Fig. 7a, the lines corresponding to the hydrodynamic equation start from a high Fr . The calculated impact pressure initially increases as Fr decreases (implying this region is dominated by increasing flow density; see Figs. 4b and 5c). The calculated impact pressure then decreases with Fr until the centre of the flow, after which Fr increases again (Fig. 4a). Only the α value of 2 intersects the peak pressure obtained using DEM, implying that an α of unity is insufficient for granular flows impacting rigid barriers. This suggests that static deposition is a crucial consideration in flow-structure interaction problems (Ng et al. 2017). The intersection occurs during the first 5% of the flow. The calculated pressure using Eqn. 4 produces a sharper increase as Fr decreases (than for Eqn. 3), but also intersects the pressure obtained using DEM during the first 5% of the flow. (Note: the data points calculated using Eqn. (4) for the body of the flow are orders of magnitude greater than the computed impact pressure. They are thus omitted for clarity.) Similar trends can be observed for each of the three lines plotted on Fig. 7b for the lower channel inclination of 14° , with the intersection occurring unambiguously within the first 5% of the flow for Eqn. 3b with $\alpha = 2$ and for Eqn. 4.

This again suggests that some of the methods used for characterising Fr are unconservative and potentially dangerous. Adopting anything but the frontal velocity and depth would cause a severe underestimate in the Fr characterised (Fig. 4a). In turn, this would lead to a mis-estimate of the impact force calculated using either Eqns. 3 or 4 (Hübl et al. 2009 and Albaba et al. 2018, respectively). This could potentially cause catastrophic failure of the barrier. Furthermore, even though Eqn. 4 explicitly states the constituent parameters involved in impact dynamics, for engineering practice, Eqn. 3 (Hübl et al. 2009) with $\alpha = 2$ may be more appropriate than Eqn. 4 (Albaba et al. 2018). This is because fewer input parameters are required, and since the pileup height and density change are not required a priori. It is also

worth noting that a wide range of values for α are reported for different flows, many of which lie outside the theoretical upper bound of 2 (see Cui et al. 2015). The wide range of values is likely due in part to improper characterisation of flow velocity and density.

Parametric study on grain diameter

The previous section sought to identify which part of a flow should be adopted for the characterisation of Fr . A single grain size was used, since the calculation of Fr is independent of grain size. However, as mentioned in the introduction, the ratio δ/h also influences flow dynamics for open-channel granular flows (Armanini 2015). In this sub-section, results from a parametric study that was carried out to assess the influence of particle size on Fr are presented.

Fig. 8a shows Fr on the ordinate and the normalised position along the flow L on the abscissa. Regions denoting transitional and supercritical Froude conditions are indicated (Faug 2015). Data corresponding to three numerical simulations with differing values of δ/B , and hence δ/h , is shown. (The value of h is defined at the thickest point of the flow.) The channel inclination is 30° for each flow. The same general trend that was shown in Fig. 4a is also observed here. For the three flows in Fig. 8a, Fr is highest at the flow front and then diminishes to a minimum near the centre of the flow. Fr then tends to increase again near the tail of the flow.

Interestingly, Fr decreases across the entire length of the flow as the grain size δ , and hence the ratio δ/h , increases. The difference is most pronounced at the head of the flow, with Fr_{\max} of 17 being recorded for $\delta/h = 0.14$, and Fr_{\max} of 6 for $\delta/h = 0.31$. The difference in Fr near the centre of the flow is much less.

The reason for this can be understood from Fig. 8b, in which normalised energy is shown on the ordinate, and L on the abscissa. Four lines corresponding to the kinetic and gravitational potential energy in the flow, for two ratios of δ/h ($\delta/h = 0.14$ and 0.31 , respectively) are shown. The lines are the specific energy at each point longitudinally along the flow normalised by the maximum energy recorded. This maximum energy occurred for the kinetic energy for the larger value of δ/h . For both

flows, the kinetic energy rapidly increases along the first part of the flow, reaches a maximum and then decreases nearly linearly. The gravitational potential energy follows a similar trend for both flows, but the maxima are much less than for the kinetic energy. The maximum kinetic energy for the larger value of δ/h is around 20% more than for the other case. However, the maximum gravitational potential energy for $\delta/h = 0.31$ is about double that of $\delta/h = 0.14$. Since the gravitational potential energy differs by proportionately more, it tends to dominate the effects of kinetic energy on Fr , hence the reduction in Fr as δ/h increases, as shown in Fig. 8a.

It is worth noting that the total kinetic and gravitational energy is higher for $\delta/h = 0.31$ than for $\delta/h = 0.14$, despite the initial gravitational potential energy being the same for both cases. This difference in energy is due to there being fewer inter-grain contacts for the larger value of δ/h . Furthermore, the inset in Fig. 8a shows normalised total flow time on the ordinate and the ratio δ/h on the abscissa. The total flow time decreases as δ/h increases; from Fig. 8b, it can be inferred that this reduction in flow time is primarily due to an increase in flow depth rather than an increase in velocity.

Fig. 8c shows the minimum Fr on the ordinate and the ratio between grain diameter and maximum flow depth δ/h on the abscissa. The minimum Fr was adopted for this graph as it is more reliably characterised than that at the flow front; nonetheless, minimum Fr is a reliable indicator of maximum Fr at the flow front (Fig. 4a). As shown in previous graph, an increase in the channel inclination leads to an increase in Fr . For channel inclinations of $\theta = 22, 30$ and 38° , there is a decrease in the minimum Fr as the ratio δ/h increases, as discussed in the previous paragraphs. By contrast, a very slight increase in Fr_{\min} is observed for $\theta = 14^\circ$, which may be a product of the very low values of δ/h for this channel inclination.

Validity of findings

As stated in the introduction, characterising Fr is difficult for unsteady flows is difficult because it varies along the length of the flow. We have therefore carried out a series of numerical simulations using a calibrated DEM model and compared runup height and impact pressure for a wide range of flows with predictions from analytical

formulae. Through this exercise, we have been able to identify the part of the flow which governs runup and impact pressure, which is a novel and important finding. The results from this study have been shown to be reliable for the simplified flow cases simulated. However, the effectiveness and reliability of these results for more complex flows (e.g. those including a liquid phase) and different scales warrants further investigation (Iverson 2015). This is especially relevant given that the results from Fig. 8c demonstrate that non-macroscopic quantities are able to affect Fr .

Conclusions

The Froude number Fr is known to govern many aspects of interaction between channelised granular flows and structures. However, there has been little agreement in the literature about how to characterise Fr for unsteady flows, where it varies substantially along the length of the flow. The present study has sought to clarify the part of the flow that should be adopted for characterising Fr .

Results from this study show that the front 5% of the flow governs both pileup height and peak impact pressure. Adopting the maximum flow thickness and velocity instead (as in Scheidl et al. 2014) would lead to values of Fr much smaller than at the flow front (Fig. 4a). Adopting such a procedure for characterising Fr could potentially lead to an under-estimate of the peak impact pressure or pileup height, since the relevant quantities for velocity, density and flow depth would be mis-estimated. Equivalently, it is also possible that error in the characterised Fr may lead to an incorrect back-calculated value for the impact coefficient α . This can cause it to be inaccurate by as much as a factor of two.

However, even though the frontmost part of the flow controls pileup height and impact pressure, it is not practical to characterise Fr there given its extreme variation longitudinally at the flow front (Fig. 4a). It may be more consistent characterisation can be achieved by taking Fr near the longitudinal centre of the flow (where the depth is maximum). Calibration curves such as Fig. 4a can then be used to extrapolate Fr at the front. This also implies that open channel tests and simulations must be complimentary to impact tests and simulations.

Acknowledgements

The authors are grateful for the financial sponsorship from the National Natural Science Foundation of China (5170091039). The authors would like to thank the support from the theme-based research grant T22-603/15N and general research fund 16209717 of Hong Kong Research Grants Council and the Hong Kong Jockey Club Charities Trust. Finally, the authors are grateful for the support of the HKUST Jockey Club Institute for Advanced Study. The authors would like to thank the financial support by the Hong Kong Jockey Club Disaster Preparedness and Response Institute (HKJCDPRI18EG01).

References

- Albaba, A., Lambert, S. and Faug, T. 2018. Dry granular avalanche impact force on a rigid wall: analytic shock solution versus discrete element simulations. *Physical Review E*, **97**: 052903.
- Arattano, M., Marchi, L., and Cavalli, M. 2012. Analysis of debris-flow recordings in an instrumented basin: confirmations and new findings. *Natural Hazards and Earth System Sciences*, **12**: 679–686. doi:10.5194/nhess-12-679-2012.
- Armanini, A. and Larcher, M. 2001. Rational criterion for designing opening of slit check dam. *Journal of Hydraulic Engineering, ASCE*, **127**(2): 94–104.
- Armanini, A., Larcher, M., and Odorizzi, M. 2011. Dynamic impact of a debris flow front against a vertical wall. *In 5th International Conference on Debris-Flow Hazards. Mitigation, Mechanics, Prediction and Assessment, Padua, Italy, 14–17 June 2011. Casa Editrice Università La Sapienza, Rome. pp. 1041–1049.*
- Armanini, A., Larcher, M., Nucci, E., and Dumbser, M. 2014. Submerged granular channel flows driven by gravity. *Advances in Water Resources*, **63**: 1–10.
- Armanini, A. 2015. Closure relations for mobile bed flows in a wide range of slopes and concentrations. *Advances in Water Resources*, **81**: 75–83.
- Ashwood, W. and Hungr, O. 2016. Estimating total resisting force in a flexible barrier impacted by a granular avalanche using physical and numerical modelling. *Canadian Geotechnical Journal* **53**(10): 1700–1717.
- Cageao, P. P. 2014. Fluid-particle interaction in geophysical flows: debris flow. PhD thesis, University of Nottingham.
- Choi, C.E., Ng, C.W.W., Song, D., Kwan, J.S.H., Shiu, H.Y.K., Ho, K.K.S. and Koo, R.C.H. 2014. Flume investigation of landslide debris baffles. *Canadian Geotechnical Journal*, **51**(5): 540–533.
- Choi, C.E., Ng, C.W.W., Song, D., Law, R.P.H., Kwan, J.S.H. and Ho, K.K.S. 2014. A computational investigation of baffle configuration on the impedance of channelized debris flow. *Canadian Geotechnical Journal*, **52**(2): 182–197.
- Choi, C. E., Au-Yeung, S. C. H. and Ng, C. W. W. 2015. Flume investigation of landslide granular debris and water runup mechanisms. *Géotechnique Letters*, **5**(1): 28–32.

- Choi, C. E., Goodwin, G. R., Ng, C. W. W., Cheung, D. K. H., Kwan, J. S. H., and Pun, W. K. 2016. Coarse granular flow interaction with slit-dams. *Géotechnique Letters* **6**: 267–274.
- Cui, P., Zeng, C. and Lei, Y. 2015. Experimental analysis on the impact force of viscous debris flow. *Earth Surface Processes and Landforms* **40**: 1644–1655.
- Eu, S., Im, S., Kim, D. and Chun, K. W. 2017. Flow and deposition characteristics of sediment mixture in debris flow flume experiments. *Forest Science and Technology*, **13**(2): 61–65, DOI: 10.1080/21580103.2017.1311949.
- Faug, T. 2015. Macroscopic force experienced by extended objects in granular flows over a very broad Froude-number range. *European Physics Journal E* **38**(5): Article 34.
- Gray, J. M. N. T., Tai, Y. C., and Noelle, S. 2003. Shock waves, dead-zones and particle-free regions in rapid granular free-surface flows. *Journal of Fluid Mechanics* **491**: 161–181.
- Hákonardóttir, K. M., Hogg, A. J., Batey, J. and Woods, A. W. 2003. Flying avalanches. *Geophysical Research Letters*, **30**(23): 2191, 1–4. DOI: 10.1029/2003GL018172.
- Hübl, J., Suda, J., Proske, D., Kaitna, R., and Scheidl, C. 2009. Debris flow impact estimation. *In Proceedings of the 11th International Symposium on Water Management and Hydraulic Engineering, Ohrid, Macedonia*, pp. 1–5.
- Hungr, O., Evans, S. G., Bovis, M. J., and Hutchinson, J. N. 2001. A review of the classification of landslides of the flow type. *Environment and Engineering Geoscience*, **7**(3): 221–238.
- Iverson, R. M. 2015. Scaling and design of debris-flow experiments. *Geomorphology*, **244**, 9–20.
- Jiang, Y., and Towhata, I. 2013. Experimental study of dry granular flow and impact behavior against a rigid retaining wall. *Rock Mechanics and Rock Engineering*, **46**(4): 713–729.
- Kloss, C., and Goniva, C. 2010. LIGGGHTS – a new open source discrete element simulation software. *In Proceedings of the 5th International Conference on Discrete Element Methods*. pp. 25–26.

- Law, P. H. 2015. Computational study of granular debris flow impact on rigid barriers and baffles. PhD Thesis, Hong Kong University of Science and Technology, Hong Kong, China.
- Ng, C. W. W., Choi, C. E., Koo, R. C. H., Goodwin, G. R., Song, D. and Kwan, J. S. H. 2017. Dry granular flow interaction with dual-barrier systems. *Géotechnique*, DOI: 10.1680/jgeot.16.P.273.
- Ng, C. W. W., Song, D., Choi, C. E., Liu, H. D., Kwan, J. S. H., Koo, C. H. and Pun, W. K. 2017. Impact Mechanisms of Granular and Viscous Flows on Rigid and Flexible Barriers. *Canadian Geotechnical Journal*, **54**(2): 188–206.
- Proske, D., Suda, J., and Hübl, J. 2011. Debris flow impact estimation for breakers. *Georisk: Assessment and Management of Risk for Engineered Systems and Geohazards*, **5**(2): 143–155.
- Sassa, K., and Wang, G. 2005. Mechanism of landslide-triggered debris flows: liquefaction phenomena due to the undrained loading of torrent deposits. In *Debris-flow hazards and related phenomena*. Springer-Berlin, Heidelberg. pp. 81–104. DOI: 10.1007/3-540-27129-5_5.
- Scheidl, C., Chiari, M., Kaitna, R., Müllegger, M., Krawtschuk, A., Zimmermann, T. and Proske, D. 2013. Analysing debris-flow impact models, based on a small-scale modelling approach. *Surveys of Geophysics*, **34**: 121–140. DOI: 10.1007/s10712-012-9199-6.
- Vagnon, F. and Segalini, A. 2016. Debris flow impact estimation on a rigid barrier. *Natural Hazards Earth Systems Science*, **16**: 1691–1697.
- VanDine, D. F. 1996. Debris flow control structures for forest engineering. (Ministry of Forests Research Program, Working Paper 22/1996). Government of the Province of British Columbia, Vancouver.
- Zhou, G. D. D., and Ng, C. W. W. 2010. Numerical investigation of reverse segregation in debris flows by DEM. *Granular Matter*, **12**: 507-516.

Figure captions:

Fig. 1: Schematic of a wedge-shaped flow front

Fig. 2: (a) Top-down image of the physical flume; (b) plan-view schematic of both the physical flume and the DEM model; (c) side-view schematic of both the physical flume and DEM model

Fig. 3: Calibration of physical (left) and numerical (right) kinematics. (a) $t = 0.0$ s; (b) $t = 0.2$ s; (c) $t = 0.4$ s; (d) $t = 0.6$ s; (e) $t = 0.8$ s

Fig. 4: Evolution of (a) open-channel Froude conditions and (b) open-channel solid volume fraction (equivalently bulk density)

Fig. 5: For a flow impacting a rigid barrier on a channel inclination of 14° and 30° , evolution of (a) impact pressure; (b) pileup height; (c) solid volume fraction (equivalently bulk density). These quantities are calculated using values recorded on the rigid barrier.

Fig. 6: Evolution of predicted pileup height based on the Froude conditions and density at each point for an open-channel flow. The data points correspond to portions of the flow, where each portion is 5% of the total flow length (i.e. $L/20$), as indicated graphically in the inset. As such, there are 20 data points for each line. No barrier was included for these tests.

Fig. 7: Normalised impact pressure calculated along the length of the flow. (a) 30° ; (b) 14° . The arrows indicate progression from the head of the flow to the tail. The data points correspond to portions of the flow, where each portion is 5% of the total flow length (i.e. $L/20$), as indicated graphically in the inset. As such, there are 20 data points for each line.

Fig. 8: (a) Froude conditions for flows at the same channel inclination with different grain diameters; (b) kinetic and gravitational energy for two grain diameters plotted as a function of L , normalised by the maximum kinetic energy (c) influence of grain diameter on minimum Fr for different channel inclinations

Froude characterisation for single-surge unsteady dry granular flows:
impact pressure and runup height

2018/07/31

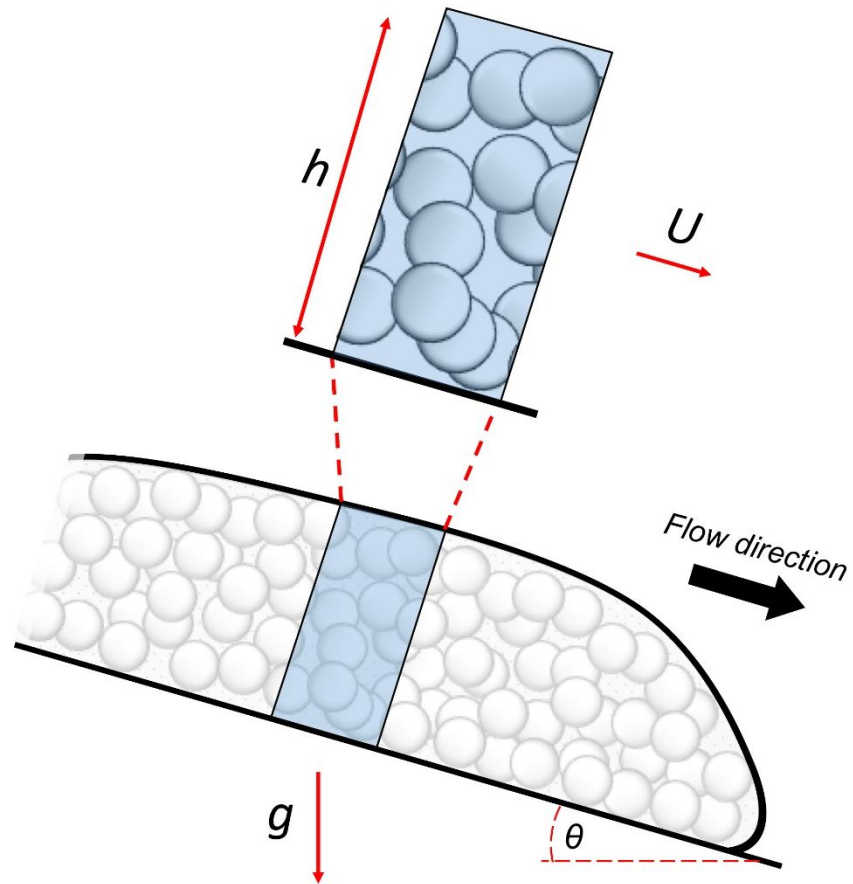


Fig. 1: Schematic of a wedge-shaped flow front

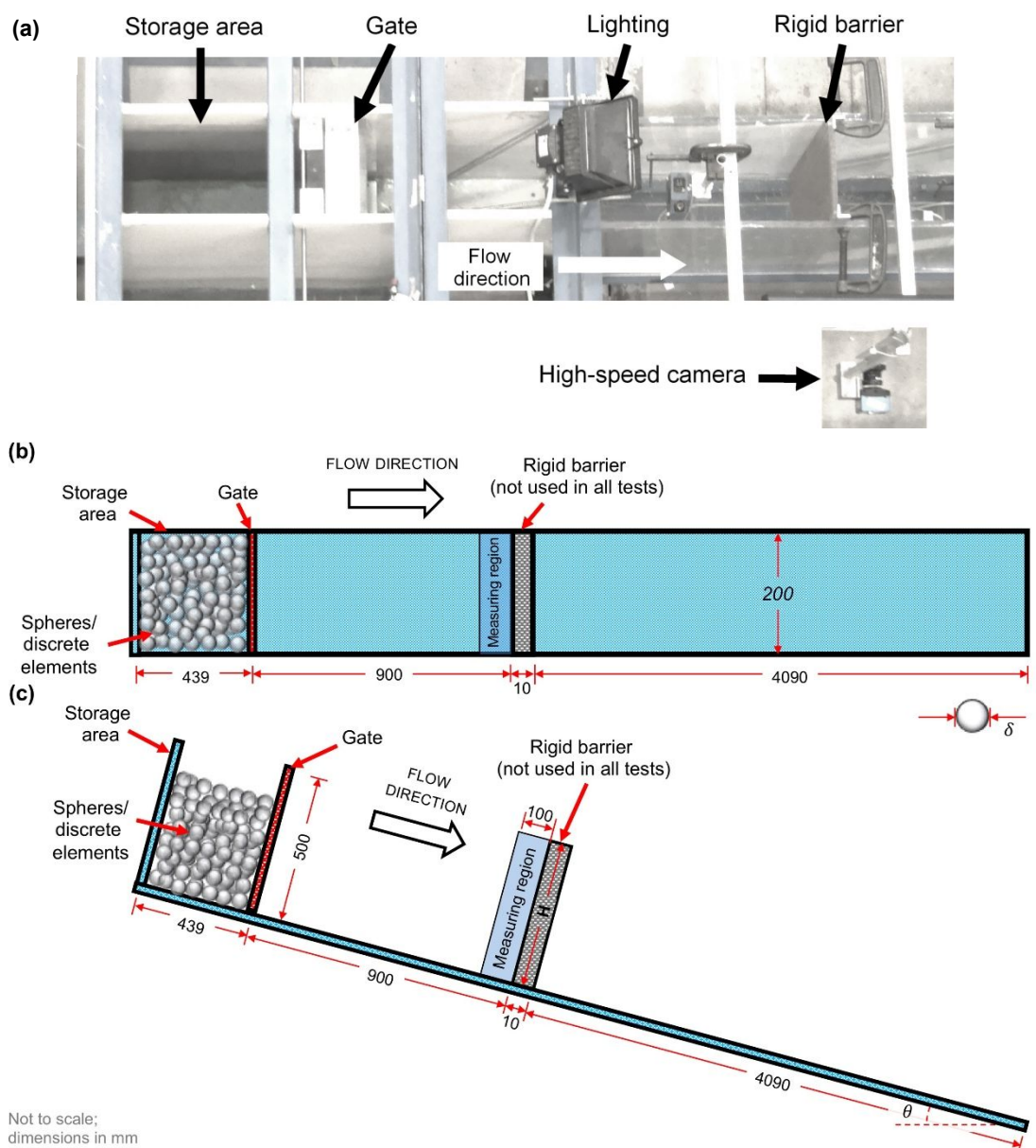


Fig. 2: (a) Top-down image of the physical flume; (b) plan-view schematic of both the physical flume and the DEM model; (c) side-view schematic of both the physical flume and DEM model

Can. Geotech. J. Downloaded from www.nrcresearchpress.com by UNIV LIBRARY OF HONG KONG UNIV OF on 06/25/19
For personal use only. This Just-IN manuscript is the accepted manuscript prior to copy editing and page composition. It may differ from the final official version of record.

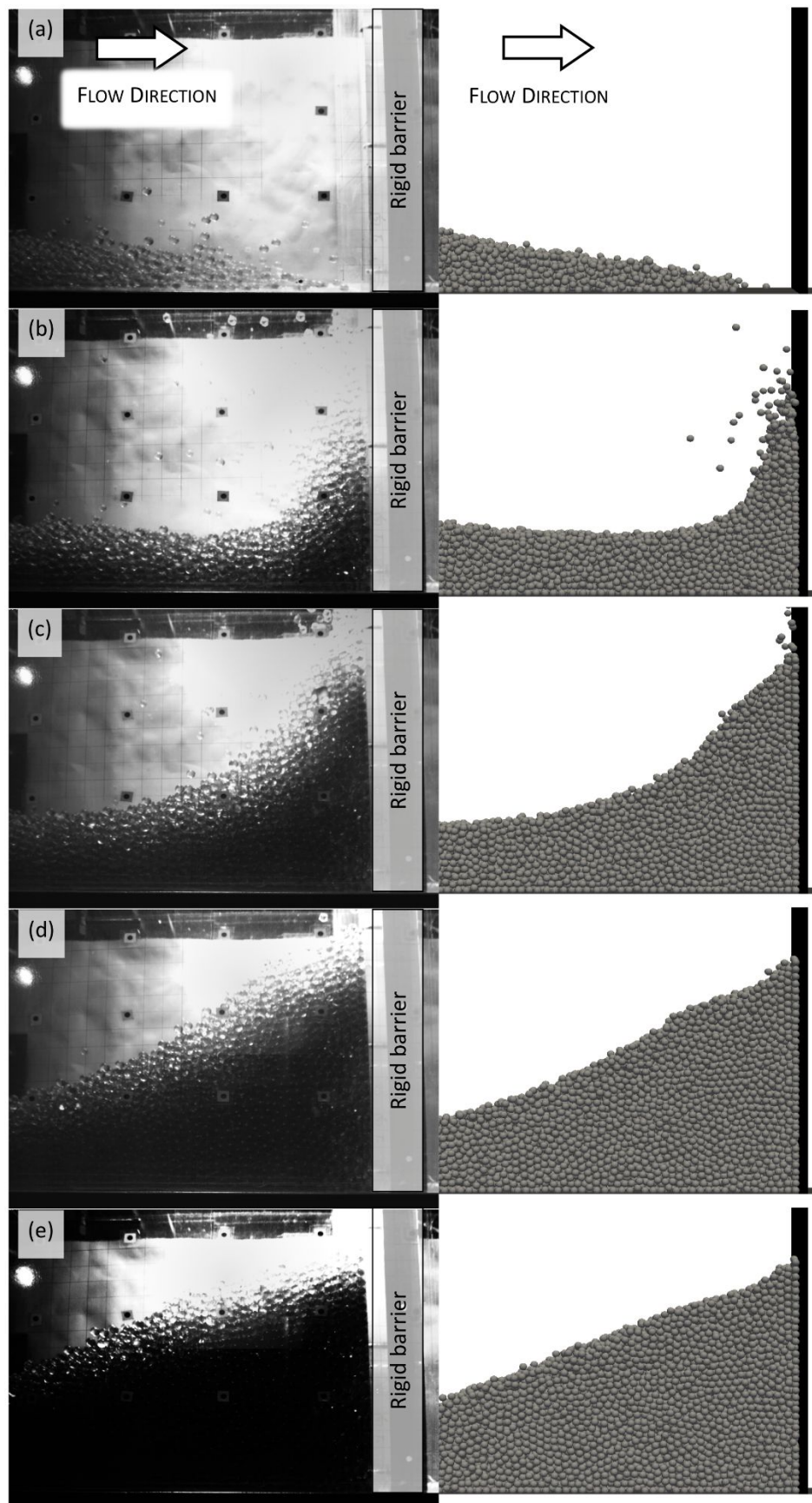


Fig. 3: Calibration of physical (left) and numerical (right) kinematics. (a) $t = 0.0$ s; (b) $t = 0.2$ s; (c) $t = 0.4$ s; (d) $t = 0.6$ s; (e) $t = 0.8$ s

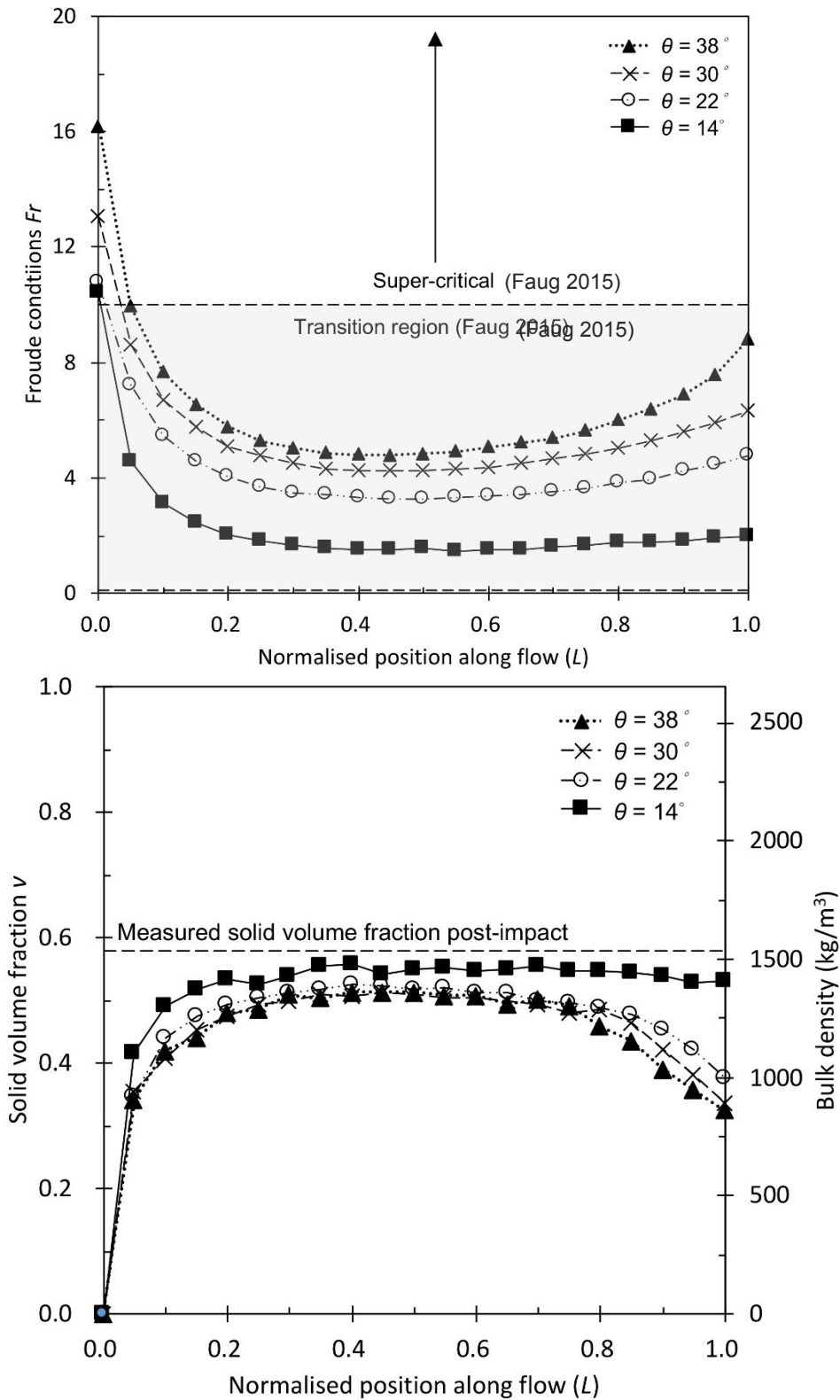


Fig. 4: Evolution of (a) open-channel Froude conditions and (b) open-channel solid volume fraction (equivalently bulk density)

Froude characterisation for single-surge unsteady dry granular flows:
impact pressure and runup height

2018/07/31

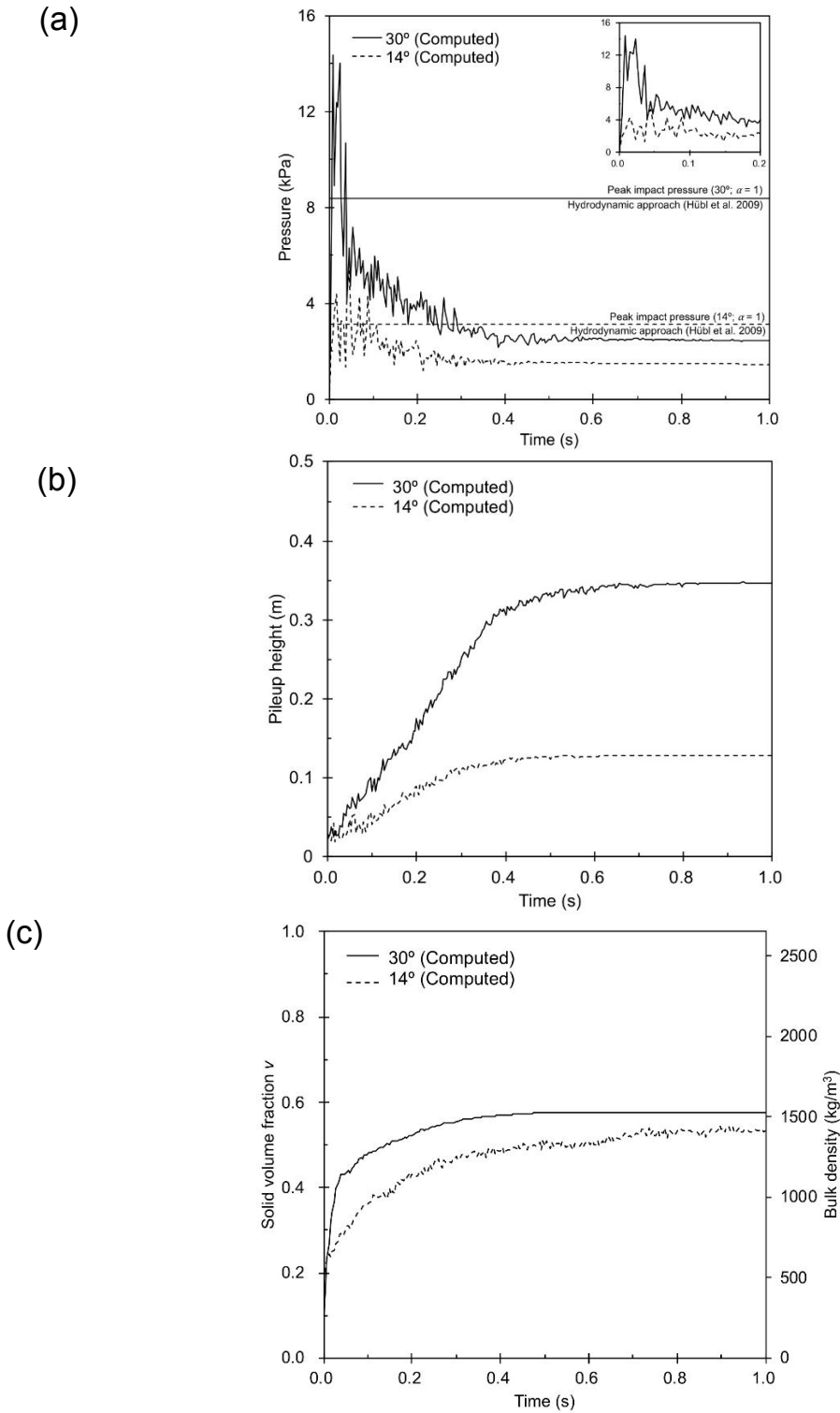


Fig. 5: For a flow impacting a rigid barrier on a channel inclination of 14° and 30°, evolution of (a) impact pressure; (b) pileup height; (c) solid volume fraction (equivalently bulk density). These quantities are calculated using values recorded on the rigid barrier.

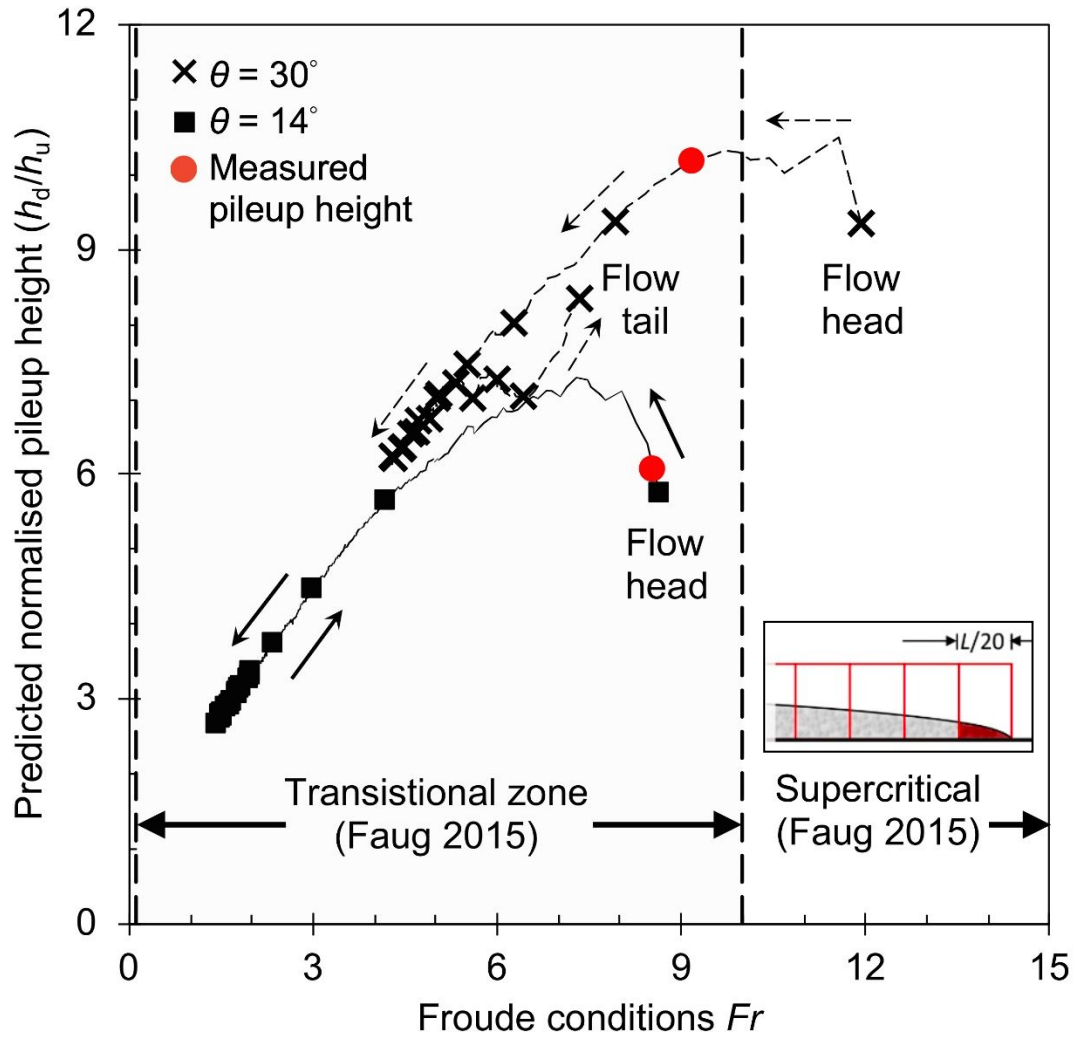


Fig. 6: Evolution of predicted pileup height based on the Froude conditions and density at each point for an open-channel flow. The data points correspond to portions of the flow, where each portion is 5% of the total flow length (i.e. $L/20$), as indicated graphically in the inset. As such, there are 20 data points for each line. No barrier was included for these tests.

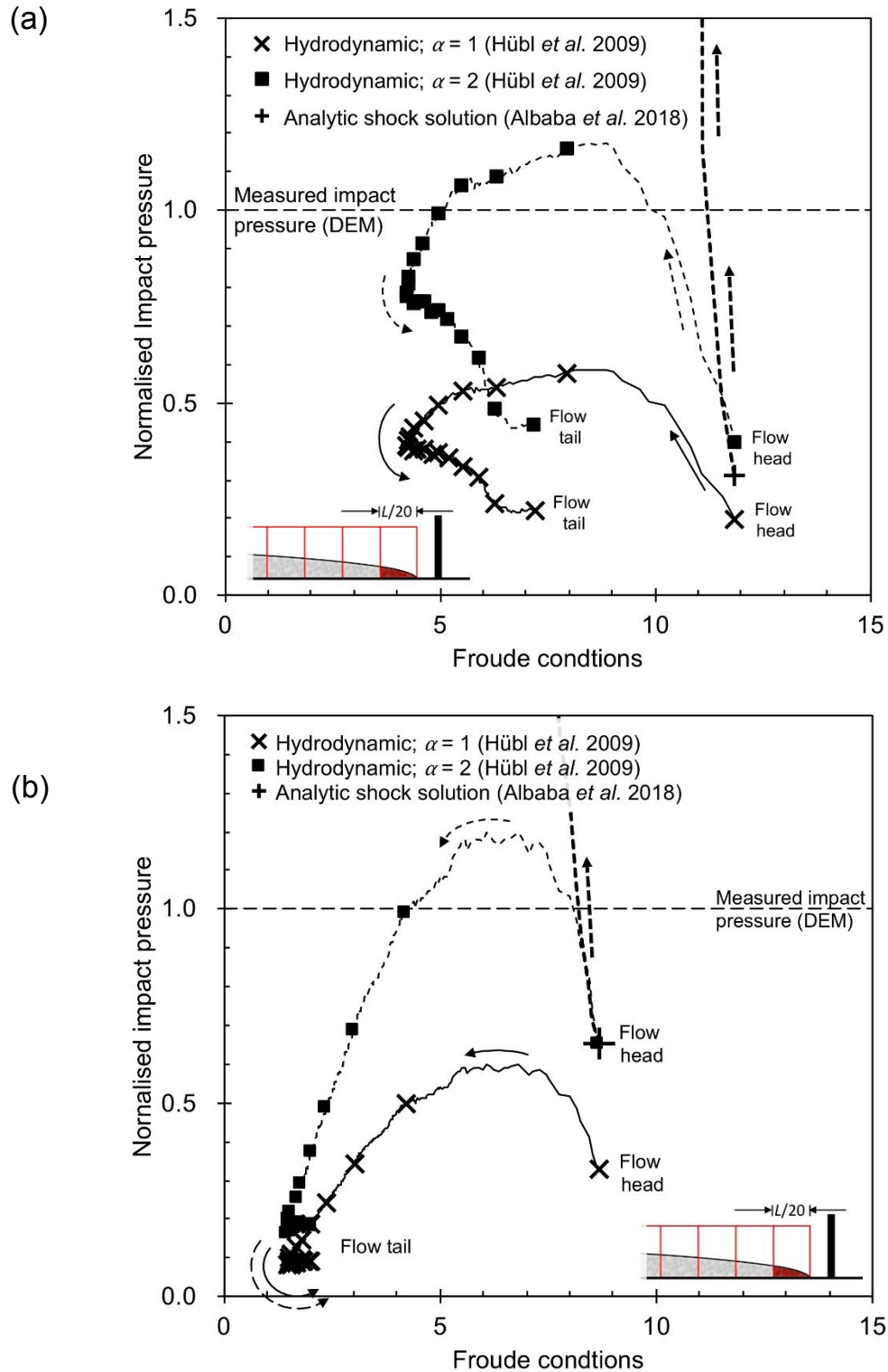


Fig. 7: Normalised impact pressure calculated along the length of the flow. (a) 30°; (b) 14°. The arrows indicate progression from the head of the flow to the tail. The data points correspond to portions of the flow, where each portion is 5% of the total flow length (i.e. $L/20$), as indicated graphically in the inset. As such, there are 20 data points for each line.

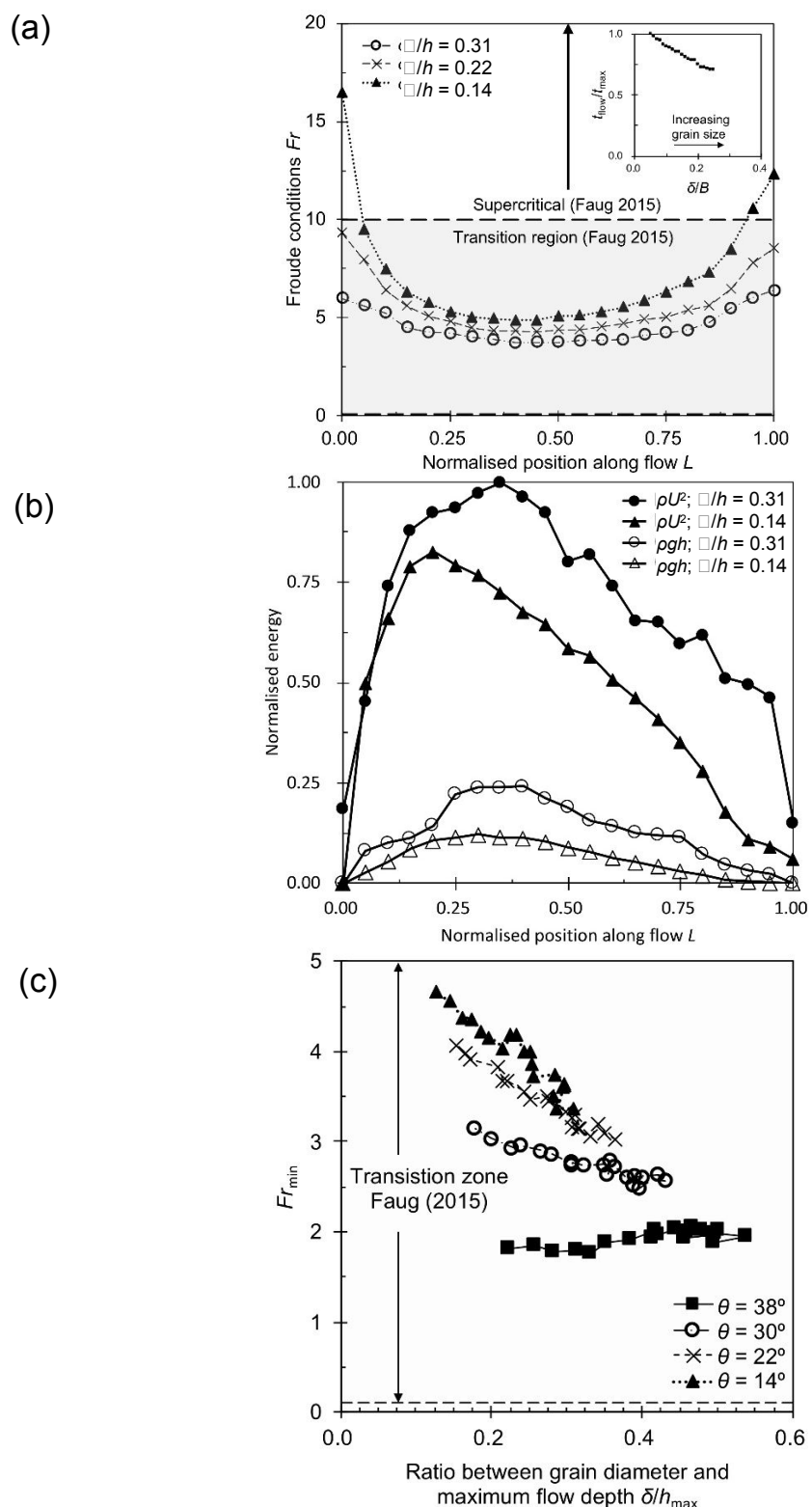


Fig. 8: (a) Froude conditions for flows at the same channel inclination with different grain diameters; (b) kinetic and gravitational energy for two grain diameters plotted as a function of L , normalised by the maximum kinetic energy (c) influence of grain diameter on minimum Fr for different channel inclinations

Can. Geotech. J. Downloaded from www.nrcresearchpress.com by UNIV LIBRARY OF HONG KONG UNIV OF on 06/25/19
For personal use only. This Just-IN manuscript is the accepted manuscript prior to copy editing and page composition. It may differ from the final official version of record.

Froude characterisation for single-surge unsteady dry granular flows:
impact pressure and runup height

2018/07/31

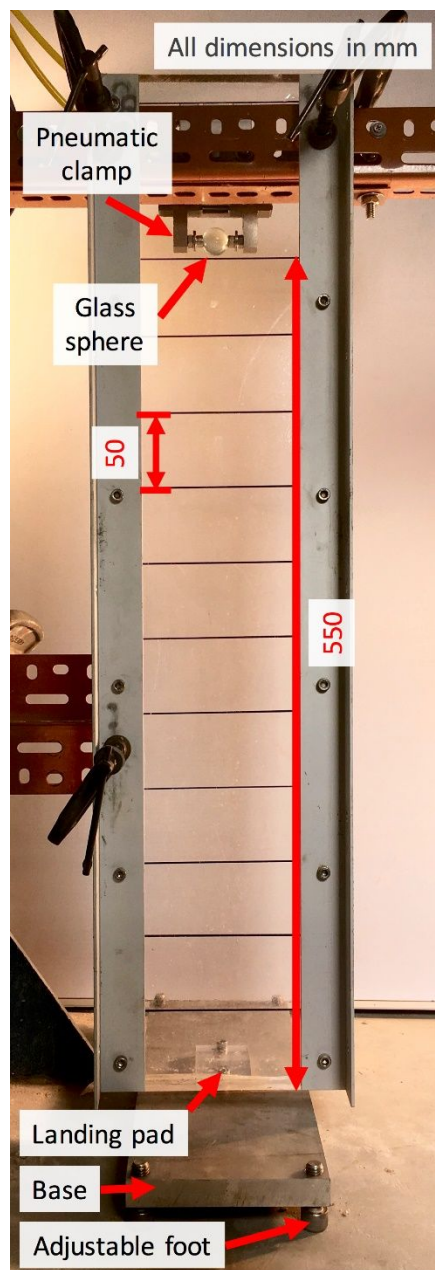


Fig. A1: Apparatus (‘the restitutor’) used to determine the coefficient of restitution for the glass beads used in the physical experiments.

Table 1: Numerical parameters

	Flume	DEM	Source
Particle diameter (m)	0.01	0.01	Measured
Total mass (kg)	40	40	Measured
Material density (kg/m ³)	2650	2650	Measured
Coefficient of restitution	0.76	0.76	Measured
Inter-grain friction coefficient	-	0.36	Calibrated
Grain-boundary friction coefficient	0.28	0.28	Measured
Young's modulus (N/m ²)	-	10 ⁸	Law 2015
Contact model	-	Hertzian	Law 2015
Timestep (s)	-	0.000005	Law 2015

Table 2: Numerical test program

Test ID	Transverse blockage	Channel inclination (°)	Grain size (mm)
T0C14	0	14	10, 12, 14 .. 46, 48, 50
T0C22	0	22	
T0C30	0	30	
T0C38	0	38	
T1C14	1	14	10
T1C30*	1	30	10

* Both physical and DEM tests performed

Appendix: Characterisation of coefficient of restitution

The coefficient of restitution characterises the amount of energy dissipated during every collision within a flow (Zhou and Ng, 2010). It is thus vital to characterise the coefficient of restitution well to capture flow dynamics accurately. The coefficient of restitution of a sample of glass spheres was determined using a series of drop tests, using specially-designed apparatus (Fig. 4). A pneumatically-controlled clamp is used to hold and subsequently release the glass sphere. A landing pad is placed directly beneath the clamp. The landing pad is tightly screwed into the metal base, such that it can be assumed to be rigid. A rigid transparent plate is clamped in front of the pneumatic clamp and landing pad. This plate is marked with lines spaced 50 mm apart to facilitate interpretation of data. The base is supported on four adjustable feet; the pneumatic clamp, the transparent plate and the landing pad were all adjusted until they were perfectly level usually a circular spirit level.

The 9.8 mm ball was dropped from the pneumatic clamp ten times. A high-speed camera placed in front of the apparatus was used to capture the maximum height to which the sphere rebounded. The coefficient of restitution was then computed for each collision:

$$e = \frac{U_2}{U_1} = \frac{\sqrt{2gh_2}}{\sqrt{2gh_1}} = \sqrt{\frac{h_2}{h_1}} \quad (\text{A1})$$

where e is the coefficient of restitution, U is the particle velocity, g is the acceleration due to the Earth's gravity, h is the maximum height of the spheres, and the subscripts 1 and 2 denote before and after collision with the landing pad respectively. A mean and standard deviation of the height to which the spheres bounced for ten tests were taken. The coefficient of restitution was found to be 0.76 ± 0.01 . This coefficient of restitution is relevant to both the base and side-walls of the flume, because they are made of the same material. The coefficient of restitution was assumed to apply to ball-ball contacts as well. Fig. 3 suggests that this assumption is reasonable, because the DEM recreates strikingly similar kinematics to the physical tests.

Figure caption:

Fig. A1: Apparatus ('the restitutor') used to determine the coefficient of restitution for the glass beads used in the physical experiments.